Atmos. Chem. Phys. Discuss., 14, 9815–9847, 2014
www.atmos-chem-phys-discuss.net/14/9815/2014/
doi:10.5194/acpd-14-9815-2014

Atmospheric Chemistry and Physics Discussions

On the role of non-electrified clouds in the Global Electric Circuit

A. J. G. Baumgaertner[1], **G. M. Lucas**[1], **J. P. Thayer**[1], **and S. A. Mallios**[2]

[1]Department of Aerospace Engineering Sciences, University of Colorado Boulder, Boulder, Colorado, USA
[2]Communications and Space Sciences Laboratory, Department of Electrical Engineering, Penn State University, University Park, Pennsylvania, USA

Received: 20 March 2014 – Accepted: 6 April 2014 – Published: 15 April 2014

Correspondence to: A. J. G. Baumgaertner (work@andreas-baumgaerner.net)

Published by Copernicus Publications on behalf of the European Geosciences Union.

Abstract

Non-electrified clouds in the fair-weather part of the Global Electric Circuit (GEC) reduce conductivity because of the limited mobility of charge due to attachment to cloud water droplets, effectively leading to a loss of ions. A high-resolution GEC model, which numerically solves the Poisson equation, is used to show that in the fair-weather region currents partially flow around non-electrified clouds, with current divergence above the cloud, and convergence below the cloud. An analysis of this effect is presented for various types of non-electrified clouds, i.e. for different altitude extents, and for different horizontal dimensions, finding that the effect is most pronounced for high clouds with a diameter below 100 km. Based on these results, a method to calculate column and global resistance is developed that can account for all cloud sizes and altitudes. The CESM1(WACCM) Earth System Model as well as ISCCP cloud data are used to calculate the effect of this phenomenon on global resistance. From CESM1(WACCM), it is found that when including non-electrified clouds in the fair-weather estimate of resistance the global resistance increases by up to 73 %, depending on the parameters used. Using ISCCP cloud cover leads to an even larger increase, which is likely to be overestimated because of time-averaging of cloud cover. Neglecting current divergence/convergence around small clouds overestimates global resistance by up to 20 %, whereas the method introduced by previous studies underestimates global resistance by up to 40 %. For global GEC models, a conductivity parametrization is developed to account for the current divergence/convergence phenomenon around non-electrified clouds. Conductivity simulations from CESM1(WACCM) using this parametrization are presented.

1 Introduction

The Global Electric Circuit (GEC) is a system of currents spanning from the troposphere to the ionosphere. Currents totaling 1–2 kA, are generated by thunderstorms,

ACPD
14, 9815–9847, 2014

which charge the ionosphere to approx. 250 kV, and return to the Earth's surface in fair-weather regions with a current density of approx. 2 pA m^{-2}. The atmosphere acts as a resistor with a global resistance of approx. 150–300 Ω. For summaries on atmospheric electricity and the GEC see e.g. Rycroft et al. (2008) and references therein.

Atmospheric electrical conductivity (the inverse of resistivity) largely determines the fair-weather current distribution and global resistance. Conductivity, σ, is proportional to the product of ion mobilities, μ^+, μ^-, and ion concentration, n:

$$\sigma = ne(\mu^+ + \mu^-), \quad (1)$$

where e is the elementary charge. Ion concentration for positive and negative ions is assumed to be equal, and is determined by the equilibrium of ion production and loss rate. Ion production in the lowermost troposphere is mostly due to radioactive decay from Radon emitted from the ground, whereas cosmic rays are the main ionization source in the upper troposphere and stratosphere. Ion-ion recombination and ion attachment to aerosols and cloud droplets lead to a loss of ions for conductivity. Detailed descriptions of conductivity are provided by Baumgaertner et al. (2013), B13 hereafter, Tinsley and Zhou (2006), TZ06 hereaffter, Rycroft et al. (2008), and Zhou and Tinsley (2010).

Non-electrified clouds in the fair-weather region, i.e. clouds that do not contribute to the source current of the GEC, have only been studied by a small number of authors. Zhou and Tinsley (2010), ZT10 hereafter, were the first to include and parametrize these clouds in global calculations of conductivity and resistance. They suggested a reduction of conductivity between one and two orders of magnitude inside the cloud. Their technique is further discussed in Sect. 5. Nicoll and Harrison (2009) presented air-to-earth current density measurements from two sites in the UK, together with solar radiation measurements, and showed that current density below the cloud can be reduced, depending on cloud height and cloud thickness. A theoretical discussion of space charge at the cloud boundaries was presented by Zhou and Tinsley (2007). A discussion of measurements of cloud edge charging from balloon flights was

ACPD
14, 9815–9847, 2014

presented by Nicoll and Harrison (2010). Zhou and Tinsley (2012) discuss time dependent charging of clouds in the fair-weather region of the GEC. A feedback of cloud edge charging on cloud evolution is discussed by Harrison and Ambaum (2009). Note that many of the studies above aimed at discussing cloud electricity in the context of speculated relevance for weather and climate. Our purpose here is to characterize the role of non-electrified clouds on the GEC by studying the current flow, potentials and resistances in the local environment of these clouds.

Cloud water droplets absorb ions, both through diffusion and conduction (Pruppacher and Klett, 1997). The effects of weakly electrified clouds can be described based on their ice and liquid droplet number concentrations and radii. Inside clouds, ion number concentration n is constrained by the equation

$$\frac{\mathrm{d}n}{\mathrm{d}t} = q - \alpha n^2 - n \sum_{i,\mathrm{r}} \beta(r_i) S(i,r) - 4\pi D n \sum_{\mathrm{r}} N_{\mathrm{r}} A_{\mathrm{r}}. \quad (2)$$

The first term on the right hand side refers to the ion pair production per unit volume, where q is the ionization rate. The second term corresponds to the ion-ion recombination, where α is the ion-ion recombination rate coefficient. The third term describes the ion attachment to neutral aerosol particles, where $\beta(r_i)$ is the attachment rate coefficient to neutral aerosol particles of type i, with radius r_i and concentration S. Finally, the last term refers to the ion attachment to cloud particles through diffusion, where N_{r} is the cloud droplet concentration, A_{r} the droplet radius, and D is ion diffusivity given by

$$D = \frac{\mu k T}{e}. \quad (3)$$

As discussed by Pruppacher and Klett (1997), for fair weather conditions the electric fields are small, such that conduction can be neglected.

For the static case considered here, Eq. (2) becomes quadratic in n. Note that Eq. (2) describes the ion attachment to cloud droplets as a loss of ions because the mobility

ACPD
14, 9815–9847, 2014

of the ionized droplets is very small, such that they are effectively lost for electrical conductivity.

From conductivity, column resistance and global resistance can be derived, which are both important parameters for the GEC. Note however that the concept of column resistance is based on the assumption of small horizontal gradients in potential and conductivity, i.e. only vertically flowing currents. Strong horizontal gradients in potential and conductivity violate this approach, as will be demonstrated in the next section.

Column resistance is defined as the vertical integration of the reciprocal of conductivity:

$$R_{\mathrm{col}} = \int_{\mathrm{surface}}^{\mathrm{ionosphere}} \frac{1}{\sigma(z)} \mathrm{d}z, \tag{4}$$

where dz are the layer thicknesses. Then, global resistance can be calculated as the horizontal integral of reciprocal column resistance:

$$R_{\mathrm{tot}}^{\mathrm{col}} = \left(\iint \frac{r^2 \cos(\lambda) \mathrm{d}\phi \mathrm{d}\lambda}{R_{\mathrm{col}}(\phi, \lambda)} \right)^{-1}, \tag{5}$$

where r is the Earth's radius, ϕ is longitude and λ is latitude.

Global models of conductivity generally do not resolve clouds. To account for a model grid cell cloud cover fraction f and a reduction of conductivity by a factor η inside a cloud, ZT10 and B13 used the law of combining resistors in parallel and derived

$$\sigma'(z) = (1 - f(z))\sigma(z) + \eta f(z)\sigma(z) \tag{6}$$

to correct for non-electrified cloud reduction of conductivity. However, the parallel resistor law can only be applied if the resistors are connected, i.e. the same potential must be present at the connection points. For a non-electrified cloud that would mean that

ACPD
14, 9815–9847, 2014

there is equal potential above the cloud-covered fraction of the grid box and above the clear-air fraction of the grid box at the same height, i.e. no horizontal potential gradient in each grid box. Analogously, no horizontal potential gradient would be allowed at the level below the cloud. With this approach it would follow that most of the fair-weather current flows around the cloud because of the large resistance of the cloud. This is depicted in Fig. 1a, showing the current flow (arrows) and average column resistance R_{col}. In Sect. 3, using a GEC model it will be shown that only for very small clouds the horizontal resistance above/below the cloud can be neglected, allowing to assume equal horizontal potential. The approach here is therefore termed the small cloud approximation. Note that ZT10 and B13 did not consider the potential changes and assumed their approximation was valid for all cloud sizes.

A different approach to account for clouds, here termed the large cloud approximation, uses the fact that the ionosphere as well as the Earth's surface both have equal potential on a scale up to the order of magnitude of 1000 km, thus on a scale applicable for cloud resistance calculations. Resistance of a column with partial cloud cover f is then estimated using the parallel resistor law:

$$\frac{1}{R_{col}} = \frac{f}{R_{col}^{cloud}} + \frac{1-f}{R_{col}^{no\text{-}cloud}} \tag{7}$$

where R_{col}^{cloud} is calculated with Eq. (4) using a conductivity profile with conductivity $\eta\sigma(z)$ for levels z with cloud cover, i.e. assuming 100 % cloud cover in the grid cell. The assumed current flow and the column resistances $R_{col}^{no\text{-}cloud}$ and R_{col}^{cloud} are depicted in the schematic of Fig. 1b. The approach can be extended to account for several layers of clouds. However, this formulation only applies when the currents are assumed to flow vertically (normal to Earth's surface). For small clouds, where currents flow around the cloud as will be shown in Sect. 3, horizontal currents arise above and below the cloud, and the approximation of Eq. (7) only holds for large clouds. For a general solution, integration would need to occur over lines of constant potential. A demonstration of the error resulting from a simple example problem can be seen in Romano and Price (1996).

ACPD
14, 9815–9847, 2014

To account for small-scale conductivity changes through clouds, global resistance cannot be calculated with integrals over conductivity, and must be derived from Ohm's law by calculating the current flowing over a boundary with a fixed potential,

$$R_{\text{tot}}^{\text{Ohm}} = \frac{\Phi_{\text{I}}}{I_{\text{tot}}} \tag{8}$$

where Φ_{I} is the ionospheric potential and I_{tot} the total GEC current, which can be calculated as the surface integral of the downward component of the air-to-earth current densities:

$$I_{\text{tot}} = \iint J_{\downarrow\text{air-to-earth}}(\phi,\lambda) r^2 \cos(\lambda) \mathrm{d}\phi \mathrm{d}\lambda. \tag{9}$$

Ionospheric potential, Φ_{I}, and current density, J, can only be calculated by solving the Poisson equation for the GEC. Then, non-electrified clouds of all sizes are completely accounted for in the estimate of global resistance. However, global 3-D models of the GEC are generally not employed on spatial resolutions that resolve clouds, similar to conductivity models or climate models. Therefore, an approach is presented here that is based on replacing column resistance by an "effective column resistance" $\widehat{R}_{\text{col}}$, which can truly account for any type of clouds in the column, yielding the true global resistance $R_{\text{tot}}^{\text{Ohm}}$ by integrating over $\widehat{R}_{\text{col}}$ as in Eq. (5). This new approach is termed the Poisson approach, as the Poisson equation is solved to derive the current distribution in the vicinity of the cloud using a local area, high resolution model.

We define $\widehat{R}_{\text{col}}$ as

$$\widehat{R}_{\text{col}}(\phi,\lambda) = \frac{\Phi_{\text{I}}}{J_{\downarrow\text{air-to-earth}}(\phi,\lambda)} \tag{10}$$

ACPD
14, 9815–9847, 2014

because then, making use of the definitions in Eqs. (5), (8) and (9),

$$R_{\mathrm{tot}}^{\mathrm{col}} = \left(\iint \frac{r^2 \cos(\lambda) \mathrm{d}\phi \mathrm{d}\lambda}{\widehat{R}_{\mathrm{col}}(\phi, \lambda)} \right)^{-1} \tag{11}$$

$$= \Phi_{\mathrm{I}} \cdot \left(\iint J_{\downarrow \text{air-to-earth}}(\phi, \lambda) \cdot r^2 \cos(\lambda) \mathrm{d}\phi \mathrm{d}\lambda \right)^{-1} \tag{12}$$

$$= \frac{\Phi_{\mathrm{I}}}{I_{\mathrm{tot}}} = R_{\mathrm{tot}}^{\mathrm{Ohm}}. \tag{13}$$

With this new definition, horizontal integration of the reciprocal effective column resistance yields the global resistance $R_{\mathrm{tot}}^{\mathrm{Ohm}}$ for any type of circuit between the ground and the ionosphere, and will be used to derive the net effect of non-electrified clouds on the GEC. For the Poisson approach, Fig. 1c depicts a schematic of the current flow around the cloud, here termed the divergence/convergence phenomenon, and the "effective column resistance" $\widehat{R}_{\mathrm{col}}$, which is a function of latitude and longitude.

For the discussion of global resistance it is also important to note that for deriving time-averaged global resistance $\overline{R}_{\mathrm{tot}}$, time-averaging has to be performed over global resistance, $R_{\mathrm{tot}}(t)$, and not over conductivity or column resistance. This is due to the fact that parallel column resistances are averaged according to the parallel resistor law to derive global resistance. For example, first averaging cloud fractions $f(t)$ over time to derive $\overline{f}$ and then using $\overline{f}$ to calculate conductivity, column resistance and global resistance leads to an overestimation of global resistance. This will be discussed further in the discussion below.

Section 2 describes the conductivity module and a GEC model that is used to quantify the effects on currents and potentials. In Sect. 3, high-resolution GEC simulations of individual non-electrified clouds are presented. The effect of these findings on a global scale is discussed in Sect. 4. Section 5 develops and evaluates a parametrization of non-electrified clouds for use in conductivity models.

ACPD
14, 9815–9847, 2014

2 Model and dataset descriptions

2.1 GEC model

The potential distribution for a given conductivity distribution can be determined by solving Poisson's equation for the GEC,

$$-\nabla \cdot [\sigma \nabla \Phi] = S, \tag{14}$$

where Φ is the potential, σ is the conductivity, and S the source distribution, which describes thunderstorms and electrified clouds. The solution also yields the current density distribution J,

$$J = -\sigma \nabla \Phi. \tag{15}$$

Here, we employ a finite element model formulation, which requires a variational formulation of the partial differential equation. Incorporating boundary conditions, the problem can be written as:

$$\begin{aligned} &-\nabla \cdot [\sigma \nabla \Phi] = S \quad \text{in } \Omega, \\ &\Phi = \Phi_E \quad \text{on } \Gamma_E, \\ &\sigma \nabla \Phi \cdot n = 0 \quad \text{on } \Gamma_L \text{ and } \Gamma_R, \end{aligned} \tag{16}$$

where Γ_E is the earth boundary, and a Dirichlet boundary condition is implemented with Φ_E, the fixed potential of the earth. Γ_L and Γ_R represent the left and right boundaries of the domain where the current is expected to be vertical far away from any clouds. For the top boundary to the ionosphere, Γ_I, a Neumann boundary condition can be chosen:

$$\nabla \Phi \cdot n = 0 \quad \text{on } \Gamma_I. \tag{17}$$

ACPD
14, 9815–9847, 2014

Alternatively, it is possible to use a Dirichlet boundary condition:

$$\Phi = \Phi_I \quad \text{on } \Gamma_I. \tag{18}$$

For the GEC cloud simulations presented in the next section we specify a fixed potential and define the sources S to be zero.

The solution is obtained over the domain Ω where σ varies exponentially in height, and within Ω_C (the cloud) $\sigma_c = \eta\sigma$, where η is a constant.

The variational form of Poisson's equation solves for $\Phi \in V$, where V is a suitable function space, such that

$$a(\Phi, v) = L(v) \; \forall \; v \in V, \tag{19}$$

and

$$\begin{aligned} a(\Phi, v) &= \int_{\Omega \setminus \Omega_C} \sigma \nabla\Phi \cdot \nabla v \mathrm{d}x + \int_{\Omega_C} \sigma_c \nabla\Phi \cdot \nabla v \mathrm{d}x \\ L(v) &= \int_{\Omega} S v \mathrm{d}x \end{aligned} \tag{20}$$

where integrals over the Γ_L and Γ_R boundaries would appear in $L(v)$ if they were non-zero.

This formulation was implemented in the Fenics Python program (Logg et al., 2012) to obtain the potential and current distribution throughout the domain.

With the current densities known throughout the domain, one can integrate over the lower boundary to determine the total current

$$I_{\text{tot}} = \int_{\Gamma_E} -\sigma \nabla\Phi \mathrm{d}s. \tag{21}$$

Then, one can determine the global resistance following Eq. (8).

ACPD
14, 9815–9847, 2014

2.2 Conductivity model

Conductivity calculations are performed using the Whole Atmosphere Community Climate model (Marsh et al., 2013) which is part of the Community Earth System Model, CESM1(WACCM), with an additional module to calculate conductivity. The driving parameters in the conductivity module are temperature, density, pressure, aerosol concentrations (from CESM1(WACCM) simulations with CARMA), and optionally cloud coverage. The model is described and evaluated in detail within B13, using average atmospheric and solar conditions. Here, we use Specified Dynamics version of WACCM (SD-WACCM), where temperatures and winds are nudged to meteorological assimilation analysis results (GEOS5), see Lamarque et al. (2012) for a description.

2.3 ISCCP dataset

The ISCCP (International Satellite Cloud Climatology Project) uses data from a suite of weather satellites. We use the ISCCP cloud type classification and the associated mean annual cloud coverage data, which is derived from daytime measurements. ISCCP classifies clouds in three altitude regimes (up to 680 hPa, between 440 and 680 hPa, and above 40 hPa), and further into cumulus, stratocumulus, stratus (low clouds), altocumulus, altostratus, nimbostratus (middle clouds), and cirrus, cirrostratus, deep convection (high clouds).

Unfortunately, ISCCP does not provide global cloud thickness data. Cumulus/stratocumulus and stratus clouds were chosen to span the height range 1–2 km, altostratus to span 3–5 km, altocumulus to span 2–3 km, nimbostratus to span 2–5 km, and cirrus/cirrostratus to span 8–9.5 km. Deep convective clouds are not considered, as they are generally electrified. Other cloud categories, especially nimbostratus, might also experience electrification, but since there is not enough consistent understanding of electrified nonthunderstorm clouds (MacGorman and Rust, 1998), they will be considered non-electrified in the global resistance estimates below. However, further work

ACPD
14, 9815–9847, 2014

appears necessary for a better classification of electrified and non-electrified clouds. This will be discussed further in Sect. 5.

3 Single clouds

For the GEC simulations, an average background (cloud-free) conductivity profile from the work by B13 is used with no horizontal variability. The ionospheric potential was fixed to 300 kV at 60 km, and the earth's potential set to zero. The domain borders in the horizontal were chosen to be sufficiently far away from the cloud edge, so the domain size increases for simulations with larger horizontal cloud sizes. To simulate the effect of a single cloud, conductivity is reduced inside the cloud. As previously shown by Zhou and Tinsley (2010), the conductivity reduction inside a cloud can be approximated by a fraction η of ambient conductivity. Estimates for η range from 1/10 (Nicoll and Harrison, 2009) to 1/50 (Zhou and Tinsley, 2010).

Figures 2 and 3 present (a) the current density distribution, (b) air-to-earth current densities, (c) column resistances and (d) potential differences for a simulation of a cirrus cloud (Fig. 2) and a stratus cloud (Fig. 3). For both cases a cloud diameter of 10 km was chosen, and $\eta = 1/50$.

For the cirrus cloud a thickness of 1.5 km, spanning from 8 to 9.5 km was chosen. The top panel in Fig. 2 depicts the current streamlines with total current density. As expected, there is a strong reduction from an average current density of 2.5 pA m^{-2} to 0.6 pA m^{-2} inside the cloud. However, the streamlines show that currents bend around the cloud, leading to higher-than-average currents (red) at the edges. There is a current divergence above the cloud, and convergence below. The effect on the air-to-earth current density is shown in panel (b). The red line depicts the air-to-earth current densities if only vertical currents were permitted, i.e. the ionospheric potential divided by the column resistance R_{col}. The blue line shows the model result, indicating that the current density reduction is in fact less severe, but spread out several kilometers past the cloud edge.

ACPD
14, 9815–9847, 2014

In panel (c), showing column resistance, the red line depicts the vertically integrated column resistance R_{col}, and the blue line depicts the column resistance $\widehat{R}_{\mathrm{col}}$ calculated as ionospheric potential divided by simulated air-to-earth current density, as defined in Eq. (10) (see also the schematic in Fig. 1).

Panel (d) depicts the potential distribution around the cloud. Clearly, even for the 10 km cloud shown here, there is a strong horizontal potential gradient both above (at 9.5 km) and below (at 8 km) the cloud, showing that the assumption of the small cloud approximation of equal potential at equal heights does not hold, as mentioned in the introduction.

In order to simplify further studies of cloud effects on larger horizontal domains, it is desirable to replace $\widehat{R}_{\mathrm{col}}$ with only one value for the cloud area, where the fair-weather column resistance remains unchanged. Therefore, we are looking for a new cloud column resistance value $\widehat{R}^{\mathrm{cloud}}_{\mathrm{col}}$, that takes into account the partial current flow around the cloud. Because of the divergence/convergence of currents around the cloud, $R^{\mathrm{cloud}}_{\mathrm{col}}$ (red line) does not give the correct average cloud column resistance.

It is also possible to formulate this using current density, where the air-to-earth current density is replaced with a fair-weather current density, and a cloud current density $\widehat{J}^{\mathrm{cloud}}_{\mathrm{air\text{-}to\text{-}earth}}$, because then

$$\widehat{R}^{\mathrm{cloud}}_{\mathrm{col}} = \frac{\Phi_{\mathrm{I}}}{\widehat{J}^{\mathrm{cloud}}_{\mathrm{air\text{-}to\text{-}earth}}}. \tag{22}$$

The approach is depicted in Fig. 2b. By integrating $J^{\mathrm{no\text{-}cloud}}_{\mathrm{air\text{-}to\text{-}earth}} - J_{\mathrm{air\text{-}to\text{-}earth}}$ over the shown domain, i.e. the difference between the blue line and the fair-weather current density (green and blue areas), and dividing only by the area of the cloud, the current density reduction is attributed to the cloud area (indicated by arrows). So we define the cloud current density $\widehat{J}^{\mathrm{cloud}}_{\mathrm{air\text{-}to\text{-}earth}}$ as

$$\widehat{J}^{\mathrm{cloud}}_{\mathrm{air\text{-}to\text{-}earth}} = J^{\mathrm{no\text{-}cloud}}_{\mathrm{air\text{-}to\text{-}earth}} - A^{-1} \iint \left(J^{\mathrm{no\text{-}cloud}}_{\mathrm{air\text{-}to\text{-}earth}} - J_{\mathrm{air\text{-}to\text{-}earth}}(\phi, \lambda) \right) \mathrm{d}\phi \mathrm{d}\lambda \tag{23}$$

ACPD
14, 9815–9847, 2014

where A is the area of the cloud. The resulting current density is shown as the green line in Fig. 2b.

The green line in panel (c) of Fig. 2 shows the resulting column resistance $\widehat{R}_{\mathrm{col}}^{\mathrm{cloud}}$ using Eq. (22). This is the average cloud column resistance while accounting for the off-vertical currents. Equivalently to $\widehat{J}_{\mathrm{air\text{-}to\text{-}earth}}^{\mathrm{cloud}}$, $\widehat{R}_{\mathrm{col}}^{\mathrm{cloud}}$ can also be calculated directly. However, horizontal averaging of column resistances requires to use reciprocal column resistance. Then, $\widehat{R}_{\mathrm{col}}^{\mathrm{cloud}}$ is

$$\widehat{R}_{\mathrm{col}}^{\mathrm{cloud}} = \left(A^{-1} \iint \left(\frac{1}{\widehat{R}_{\mathrm{col}}(\phi,\lambda)} - \frac{1}{R_{\mathrm{col}}^{\mathrm{no\text{-}cloud}}} \right) \mathrm{d}\phi \mathrm{d}\lambda + \frac{1}{R_{\mathrm{col}}^{\mathrm{no\text{-}cloud}}} \right)^{-1} \tag{24}$$

which is mathematically equivalent to the previous definition of $\widehat{R}_{\mathrm{col}}^{\mathrm{cloud}}$. $\widehat{R}_{\mathrm{col}}^{\mathrm{cloud}}$ is also shown in the schematic of Fig. 1c. It is important to note that all derived column resistance values are independent of the ionospheric potential chosen for the simulation.

The results for a stratus cloud with a vertical thickness of 1.5 km and a diameter of 10 km are shown in Fig. 3. Above the cloud, a similar behavior of current spreading towards the cloud edges is found. However, since the cloud is close to the ground, the air-to-earth current density is reduced to a value similar from what would be expected if horizontal currents were neglected, as shown in panel (b). It is interesting to note that this leads to an increase in air-to-earth current density in the cloud-free area next to the cloud edges. Analogously, panel (c) shows the column resistances from vertical integration of the reciprocal of conductivity R_{col} (red), the effective column resistance $\widehat{R}_{\mathrm{col}}$ (blue), and the average column resistance $\widehat{R}_{\mathrm{col}}^{\mathrm{cloud}}$ (green) as defined above. Similarly to the cirrus cloud, the potential distribution in Fig. 3d depicts large horizontal gradients.

Note that the results are approximately independent of the vertical and horizontal resolution of the simulation, as long as the cloud and the region below the cloud are resolved.

To compare the current divergence/convergence effect for different cloud types and horizontal dimensions, we compute the ratio $\widehat{R}_{\mathrm{col}}^{\mathrm{cloud}}/R_{\mathrm{col}}^{\mathrm{cloud}}$, shown in Fig. 4, as a

ACPD
14, 9815–9847, 2014

function of cloud diameter for a variety of cloud types. Here, cloud types are only distinguished by their altitude regime, using the ISCCP types. In the future, results from other satellite missions such as the NASA ICEsat (Ice, Cloud, and land Elevation Satellite) and CloudSat missions, can be used for more accurate global cloud thickness analysis.

From Fig. 4, one can see the effect is most important for clouds with a diameter less than 100 km. In the transition range, between 2 and 100 km, generally the effect is more pronounced, i.e. a smaller $\widehat{R}_{\mathrm{col}}^{\mathrm{cloud}}/R_{\mathrm{col}}^{\mathrm{cloud}}$, for clouds with a high cloud bottom for which the current divergence/convergence becomes more important as seen above. For example, the effect is less pronounced for cumulus and stratocumulus (red) with a bottom height of 1 km than it is for altostratus (green) with a bottom height of 3 km. However, very high clouds such as the cirrus type have a smaller effect on column resistance because of the exponential increase of conductivity with altitude, i.e. changes in conductivity at higher altitudes are less important for column resistance than the same fractional change at lower altitudes. For Fig. 4 this leads to a larger ratio of $\widehat{R}_{\mathrm{col}}^{\mathrm{cloud}}/R_{\mathrm{col}}^{\mathrm{cloud}}$ for cirrus clouds (black).

A sensitivity analysis using $\eta = 1/25$ (not shown) yields increases in the ratio $\widehat{R}_{\mathrm{col}}^{\mathrm{cloud}}/R_{\mathrm{col}}^{\mathrm{cloud}}$ of approx. 0.1 for small clouds, except for cirrus where an increase of approx. 0.2 is found.

4 Global effect

For estimating the impact of non-electrified clouds on global resistance, it is necessary to take into account the cloud size distribution. Wood and Field (2011) have used MODIS, airplane and model data to show that the cloud chord length as well as the projected area obey a power law. For the cloud cover contribution C from clouds larger than $x/x_{\max}$ they showed that

$$C(x) = 1 - (x/x_{\max})^{2-\beta} \tag{25}$$

and found that $\beta \approx 1.7$ and $x_{\max} = 2000$ km.

ACPD
14, 9815–9847, 2014

The contribution C_h of any chosen set of cloud horizontal sizes h_i for the intervals $[(h_{i-1}+h_i)/2, (h_{i+1}+h_i)/2]$ can then be calculated.

If we assume this result to be true individually for all types of clouds, the size-dependent cloud cover fraction is then $g(h_i, \text{type}) = f(type) \cdot C_h(h_i)$, where cloud-cover fraction f is given by satellite observations, e.g. by ISCCP, or model simulations.

The high-resolution simulations for single clouds in the previous section are used to derive the ratio $\widehat{R}_{col}^{cloud}/R_{col}^{no\text{-}cloud}$ for every cloud type. Note that the result will be independent of the model source currents or the ionospheric potential.

The values for $R_{col}(\phi, \lambda)$, from observations or model data, are then used to derive $\widehat{R}_{col}^{cloud}$ for every cloud type. The Poisson approach column resistance $\widetilde{R}_{col}$ for a cloud-covered model or observation column can then be calculated by averaging the individual values for $\widehat{R}_{col}^{cloud}(h_i, \text{type})$ weighted by the corresponding cloud cover fraction:

$$\widetilde{R}_{col} = \left(\sum_{\text{i, type}} \left(\widehat{R}_{col}^{cloud}(h_i, \text{type}) \right)^{-1} \cdot g(h_i, \text{type}) + \left(R_{col}^{no\text{-}cloud} \right)^{-1} \cdot \left(1 - \sum_{i,\text{type}} g(h_i, \text{type}) \right) \right)^{-1} . \quad (26)$$

The use of $\widetilde{R}_{col}$ as column resistance for a column partially covered with clouds is also visualized in Fig. 1d.

Using the ISCCP cloud cover distributions we estimate the effect on global resistance. Background (cloud-free) conductivity data was obtained from the CESM1(WACCM) simulation used below, for annual mean conditions. Table 1 lists global resistance values for a cloud-free atmosphere, the small cloud approximation, the large cloud approximation, the Poisson approach, and total cloud cover averages. Using the small cloud approximation and ISCCP cloud cover data ZT10 estimated an increase of global resistance through clouds by about 18 Ω, similar to the 22 Ω here ($\eta = 1/50$).

ACPD
14, 9815–9847, 2014

The large cloud approximation leads to increases of global resistance by up to 188 Ω (114 %), whereas with the Poisson approach, taking the current divergence/convergence into account, increases global resistance by 144 Ω (87 %). As expected, the latter value lies between the small and large cloud approximations. For $\eta = 1/50$, the small cloud approximation underestimates total resistance by 39 %, whereas the large cloud approximation overestimates it by 14 %.

Similar to ISCCP, the Earth System Model CESM1(WACCM) was also used to calculate global resistances, using the model cloud cover, which is provided as a function of altitude and horizontal location. There is no information on cloud type in CESM1(WACCM). Therefore, the cloud fractions were grouped to the same three heights as used in ISCCP (see Sect. 2.3). Then, the same procedure as for ISCCP can be used to derive column resistances.

Again, the large cloud approximation overestimates global resistance significantly, by up to 21 %, when compared to the Poisson approach.

Despite the slightly larger total cloud cover, the CESM1(WACCM) global resistances are consistently smaller by up to 37 Ω compared to ISCCP for all η. There are several reasons for the discrepancies: first, since the model provides cloud coverage as a function of altitude, there is a major difference in the treatment of cloud thickness compared to ISCCP. Secondly, ISCCP cloud coverage data is only for daytime, which can be significantly different to nighttime coverage. Finally, CESM1(WACCM) uses instantaneous values of cloud cover to calculate conductivity, column resistance, whereas ISCCP only provides time-averaged cloud cover, and therefore the derived global resistance is overestimated, as mentioned in the introduction.

The annual mean column resistances, similar to Fig. 7 in B13, are shown in Fig. 5 for ISCCP and CESM1(WACCM). Surprisingly, the model shows areas of higher column resistance in areas of high cloud coverage, yet the global resistance is smaller than from ISCCP, driven by the areas of little cloud coverage, i.e. small column resistance.

The only available measurements of air-to-earth current density depending on cloud coverage were presented by Nicoll and Harrison (2009). The authors found little change

ACPD
14, 9815–9847, 2014

in the current density measurements, only fully-overcast conditions with thick clouds led to current density reductions. The model simulations support and explain these findings. Unfortunately, the authors did not present their results as a function of cloud size, since such data was not available, so a quantitative comparison or evaluation of the model results is not possible.

5 Parametrization for 3-D conductivity calculations

3-D models used to calculate conductivity generally cannot resolve clouds because of their coarse horizontal resolution, and instead operate on cloud cover fractions for each grid box. For the calculation of conductivity in such models, a parametrization is then required to account for the effect of non-electrified clouds. The 3-D conductivity model results can then be used for global GEC models that solve Poisson's equation to derive global distributions of potentials and currents.

ZT10 have provided a parametrization to account for clouds as discussed in the introduction. However, as shown above, the approximation only holds for very small cirrus clouds and underestimates the resistance increase through clouds significantly.

Here, we introduce a parametrization suitable for all cloud sizes and vertical extents, based on the high-resolution model results of individual clouds presented above. This will yield corrections to conductivity such that the vertical current assumption can be employed again.

In a first step, the Poisson approach column resistance $\widetilde{R}_{\mathrm{col}}$ is parametrized using the approach to calculate the global effect presented in Sect. 4. The model data required for this is the fair-weather column resistance, cloud cover fractions for the pre-defined cloud types for every model grid point, and cloud cover for every model grid point as a function of model layer $f(z)$.

ACPD
14, 9815–9847, 2014

We define effective conductivity $\widetilde{\sigma}$ such that

$$\widetilde{R}_{\mathrm{col}} = \int \frac{\mathrm{d}z}{\widetilde{\sigma}(z)}. \tag{27}$$

We assume the following relationship between $\widetilde{\sigma}$ and the cloud-free conductivity:

$$\widetilde{\sigma}(z) = (1 - f(z))\sigma(z) + \gamma f(z)\sigma(z) \tag{28}$$

where a parameter γ is introduced that will take into account the non-linearity introduced by the current divergence/convergence around the clouds. Note that γ is not an assumed constant as in the work by ZT10, see Eq. (6), but will be derived from the known value for $\widetilde{R}_{\mathrm{col}}$ for every model column.

Using the assumed form for $\widetilde{\sigma}$ from Eq. (28), we can rewrite Eq. (27) as

$$\widetilde{R}_{\mathrm{col}} = \sum_{i=1}^{n} \frac{\Delta z}{\sigma(z)(1 - f(z)(1 - \gamma))} \tag{29}$$

for n model layers with thickness Δz. Eq. (29) is a polynomial with degree n for the variable γ. Here, Newton's method is used to numerically approximate γ for the function $h(\gamma) = R - \sum \Delta z/(\sigma(1 - f(1 - \gamma))) = 0$. The first derivative is $h'(\gamma) = \sum \Delta z \sigma f/(\sigma(1 - f(1 - \gamma)))^2$. With this, the solution is iteratively approximated using $\gamma_{m+1} = \gamma_m - h(\gamma_m)/h'(\gamma_m)$.

While the polynomial in general has n number of solutions, only the largest γ is physically meaningful. For other solutions conductivity of the layer with the largest cloud cover f becomes negative. The initial guess γ_0 for the largest γ is close to where the fraction reaches singularity, $\gamma_0 = 1 - 1/\max(f) + \epsilon$. Then, Newton's method reliably converges to this solution. With γ from Eq. (28), $\widetilde{\sigma}(z)$ can then be calculated.

Figure 6 shows cloud cover (left) and conductivity (right) profiles for a single column. The parametrized (red) conductivity $\widetilde{\sigma}$ is smaller than the background exponential (black) conductivity depending on the cloud cover of that layer. The ZT10 estimate is also shown (blue), where the conductivity reduction is underestimated as discussed

ACPD
14, 9815–9847, 2014

above. The corresponding column resistance values are $R_{col}^{no\text{-}clouds} = 1.0 \times 10^{17}\,\Omega\,m^2$, and $\widetilde{R}_{col} = 2.1 \times 10^{17}\,\Omega\,m^2$. Vertically integrating the conductivity $\widetilde{\sigma}$ gives a result numerically identical to $\widetilde{R}_{col}$, as required by the parametrization.

The parametrization developed above was implemented as part of the CESM1(WACCM) conductivity module. As above, cloud cover without deep convection was used, in order to include only non-electrified clouds. As an example, the logarithm of model conductivity for a single longitude and model time is shown in Fig. 7 (top). Local reductions in conductivity correspond to the local cloud cover fraction, which is also shown (black contour lines). The bottom part depicts the column resistance with (black) and without (red) clouds.

As in the previous section, the results also depend on η as well as the assumed cloud thicknesses that are used to derive $\widehat{R}_{col}^{cloud}/R_{col}^{no\text{-}cloud}$ in the high-resolution simulation part.

The effective conductivity distribution, $\widetilde{\sigma}$, can be used for global GEC models to calculate potentials and currents, while accounting for sub-grid scale effects of non-electrified clouds.

Errors from this parametrization will be largest for areas of the globe where certain types or sizes of clouds are different to average distributions. If the cloud thicknesses are different to the assumed thicknesses, the parametrization will not give accurate results. No global measurements of these parameters are available, so an estimate of the errors made is currently not possible. The parametrization is based on the assumption that these clouds are not electrified, but if future measurements show that, in addition to deep convective clouds and some nimbostratus clouds, other cloud categories do have electrification, this could significantly alter the global resistance results. The effect of large-scale precipitation on the column resistance is also not taken into account, as such effects are not yet understood. Further uncertainties in the resistance estimate are due to possible mutual coupling of clouds if they are close to each other. Figure 8 shows current streamlines (top) and column resistance (bottom) around two clouds both with radius 20 km and between 3 and 5 km in the vertical, separated by

ACPD
14, 9815–9847, 2014

3 km in the horizontal. For this simulation, the column resistance in the area between the clouds does not reach the fair-weather column resistance, indicating mutual coupling at distances below approx. 3 km for this cloud type. The cloud distance required for mutual coupling varies by cloud type and diameter. Errors of the column resistance parametrization will be increasing if a significant fraction of small clouds experiences mutual coupling. There is currently not enough satellite data available to estimate this global effect.

6 Conclusions

Using high-resolution model simulations of current flow in the fair-weather region of the GEC, the role of non-electrified clouds was investigated. A finite element model was used to solve Poisson's equation in the vicinity of various cloud sizes and altitudes. Non-electrified clouds, which decrease electrical conductivity, in general, lead to a reduced current density beneath the cloud layer; however, the model shows that currents bend around the cloud, with current divergence above the cloud and convergence below. Below the cloud, this leads to larger current densities and effectively a smaller cloud resistivity than expected if only vertical currents were considered. Qualitatively, this agrees with published air-to-earth current density measurements. This phenomenon was found to be important especially for clouds with a diameter below 100 km, and therefore to lead to a significant error when using the classical approach to estimate global resistance, i.e. horizontally integrating over column resistance. An "effective column resistance" was introduced, which restores the possibility to derive global resistance the classical way. The Poisson approach method is based on the numerical simulations of effective column resistance for single clouds as a function of cloud size and altitude.

Using the Earth System Model CESM1(WACCM) as well as the ISCCP cloud database, the effect of clouds on global resistance, taking the divergence/convergence phenomenon into account, was estimated. Employing the Poisson approach introduced

ACPD
14, 9815–9847, 2014

here, non-electrified clouds were found to increase global resistance by up to 120 Ω (73 % of the cloud-free atmosphere resistance) in the model, depending on assumed cloud properties. Using ISCCP, increases are even larger, but overestimated because of the use of time-averaged cloud cover. A previously published small cloud approximation leads to underestimation of global resistance by up to 40 %, whereas a large cloud approximation, which only considers vertical currents and neglects divergence/convergence, leads to overestimation by up to 20 %. Current divergence/convergence around non-electrified clouds should therefore not be neglected in GEC studies. For this purpose, a parametrization was developed that corrects conductivity depending on model grid cell cloud cover, allowing to assume only vertical current flow on the scale of grid columns. However, it is emphasized that for a better quantification of the role of non-electrified clouds in the GEC many aspects will require a better understanding. This includes improving estimates of the conductivity decrease in clouds, better distinctions between current generating clouds and non-electrified clouds, and improved global cloud thickness data.

Acknowledgements. This work was supported by NSF Award AGS-1135446 to the University of Colorado under the Frontiers in Earth System Dynamics Program (FESD). The National Center for Atmospheric Research is sponsored by the National Science Foundation. We would like to acknowledge high-performance computing support from Yellowstone (Computational and Information Systems Laboratory, 2012). We have used the Ferret program (http://www.ferret.noaa.gov) from NOAA's Pacific Marine Environmental Laboratory for creating some of the graphics in this paper.

References

Baumgaertner, A. J. G., Thayer, J. P., Neely, R. R., and Lucas, G.: Toward a comprehensive global electric circuit model: Atmospheric conductivity and its variability in CESM1(WACCM) model simulations, J. Geophys. Res., 118, 9221–9232, doi:10.1002/jgrd.50725, 2013. 9817

ACPD
14, 9815–9847, 2014

Computational and Information Systems Laboratory: Yellowstone: IBM iDataPlex System (NCAR Community Computing), National Center for Atmosphric Research, Boulder, CO, available at: http://n2t.net/ark:/85065/d7wd3xhc, 2012. 9836
Harrison, R. G. and Ambaum, M. H. P.: Observed atmospheric electricity effect on clouds, Environ. Res. Lett., 4, 014003, doi:10.1088/1748-9326/4/1/014003, 2009. 9818
Lamarque, J.-F., Emmons, L. K., Hess, P. G., Kinnison, D. E., Tilmes, S., Vitt, F., Heald, C. L., Holland, E. A., Lauritzen, P. H., Neu, J., Orlando, J. J., Rasch, P. J., and Tyndall, G. K.: CAM-chem: description and evaluation of interactive atmospheric chemistry in the Community Earth System Model, Geosci. Model Dev., 5, 369–411, doi:10.5194/gmd-5-369-2012, 2012. 9825
Logg, A., Mardal, K.-A., and Wells, G. N., (Eds.): Automated Solution of Differential Equations by the Finite Element Method, Springer Berlin Heidelberg, doi:10.1007/978-3-642-23099-8, 2012. 9824
MacGorman, D. R. and Rust, W. D.: The Electrical Nature of Storms, Oxford University Press, New York, 1998. 9825
Marsh, D. R., Mills, M. J., Kinnison, D. E., Lamarque, J.-F., Calvo, N., and Polvani, L. M.: Climate Change from 1850 to 2005 Simulated in CESM1(WACCM), J. Climate, 26, 7372–7391, doi:10.1175/JCLI-D-12-00558.1, 2013. 9825
Nicoll, K. A. and Harrison, R. G.: Vertical current flow through extensive layer clouds, J. Atmos. Sol.-Terr. Phy., 71, 2040–2046, doi:10.1016/j.jastp.2009.09.011, 2009. 9817, 9826, 9831
Nicoll, K. A. and Harrison, R. G.: Experimental determination of layer cloud edge charging from cosmic ray ionisation, Geophys. Res. Lett., 37, L13802, doi:10.1029/2010GL043605, 2010. 9818
Pruppacher, H. R. and Klett, J. D.: Microphysics of Clouds and Precipitation, Kluwe Academic Publishers, Dordrecht, 2nd Edn., 1997. 9818
Romano, J. D. and Price, R. H.: The conical resistor conundrum: a potential solution, Am. J. Phys., 64, 1150–1153, doi:10.1119/1.18335, 1996. 9820
Rycroft, M. J., Harrison, R. G., Nicoll, K. A., and Mareev, E. A.: An overview of earth's global electric circuit and atmospheric conductivity, Space Sci. Rev., 137, 83–105, doi:10.1007/s11214-008-9368-6, 2008. 9817
Tinsley, B. A. and Zhou, L.: Initial results of a global circuit model with variable stratospheric and tropospheric aerosols, J. Geophys. Res., 111, D16205, doi:10.1029/2005JD006988, 2006. 9817

ACPD
14, 9815–9847, 2014

Wood, R. and Field, P. R.: The distribution of cloud horizontal sizes, J. Climate, 24, 4800–4816, doi:10.1175/2011JCLI4056.1, 2011. 9829

Zhou, L. and Tinsley, B. A.: Production of space charge at the boundaries of layer clouds, J. Geophys. Res., 112, D11203, doi:10.1029/2006JD007998, 2007. 9817

Zhou, L. and Tinsley, B. A.: Global circuit model with clouds, J. Atmos. Sci., 67, 1143–1156, doi:10.1175/2009JAS3208.1, 2010. 9817, 9826

Zhou, L. and Tinsley, B. A.: Time dependent charging of layer clouds in the global electric circuit, Adv. Space Res., 50, 828–842, doi:10.1016/j.asr.2011.12.018, 2012. 9818

ACPD
14, 9815–9847, 2014

Table 1. Annual mean GEC global resistances.

	ISCCP			CESM1(WACCM)		
	$\eta = 1/10$	$\eta = 1/25$	$\eta = 1/50$	$\eta = 1/10$	$\eta = 1/25$	$\eta = 1/50$
Cloud-free atmosphere			165 Ω			
Small cloud approximation	184 Ω	186 Ω	187 Ω			
Large cloud approximation	244 Ω	303 Ω	353 Ω	215 Ω	284 Ω	345 Ω
Poisson approach	233 Ω	277 Ω	309 Ω	196 Ω	246 Ω	285 Ω
Total cloud cover		66 %			69 %	

ACPD
14, 9815–9847, 2014

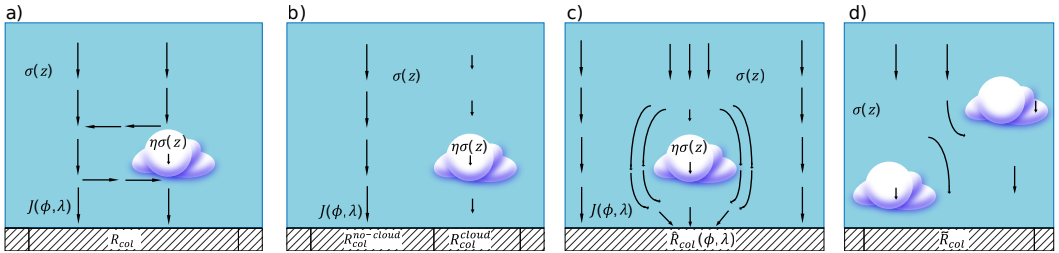

Fig. 1. Schematics of cloud modifications of conductivity and column resistance. **(a)** Single cloud, with current mainly flowing around the cloud as assumed in the small cloud approximation. **(b)** Single cloud, only allowing for vertical currents as assumed in the large cloud approximation. **(c)** Current divergence/convergence around the cloud, and "effective column resistance" as a function of latitude and longitude, employed for the Poisson approach. **(d)** Model grid column with cloud fraction and Poisson approach column resistance $\widetilde{R}_{\mathrm{col}}$.

ACPD
14, 9815–9847, 2014

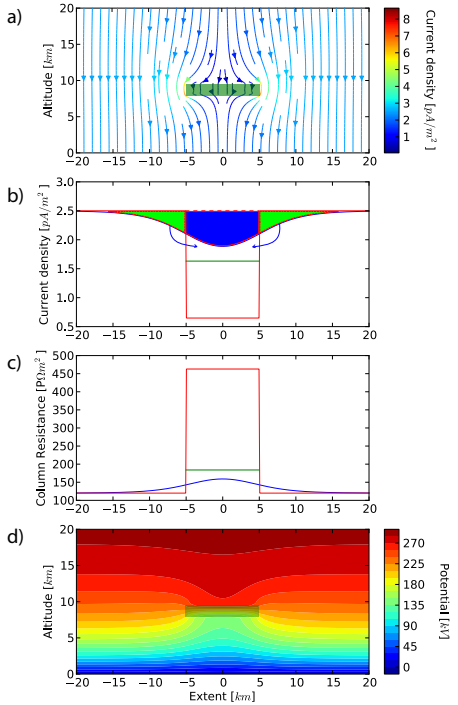

Fig. 2. (a) current streamlines and total current density around a cirrus cloud (indicated by the green box) with a diameter of 10 km, located between 8 and 9.5 km altitude. **(b)** Model air-to-earth current density (blue), restricted to vertical currents only (red). **(c)** Effective column resistance $\widehat{R}_{\mathrm{col}}$ (blue), column resistance for considering vertical currents only R_{col} (red), and mean effective cloud column resistance $\widehat{R}_{\mathrm{col}}^{\mathrm{cloud}}$ (green). **(d)** Potential difference distribution.

ACPD
14, 9815–9847, 2014

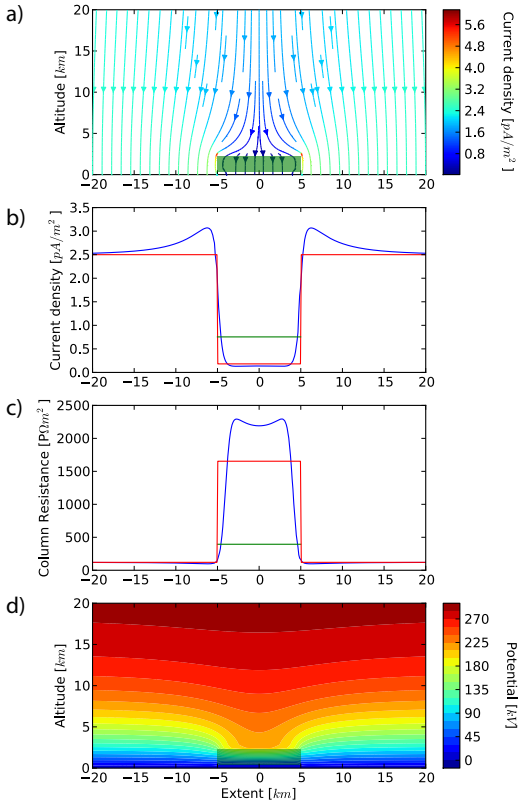

Fig. 3. As Fig. 2 but for a stratus cloud between 0.5 and 2.5 km altitude.

ACPD
14, 9815–9847, 2014

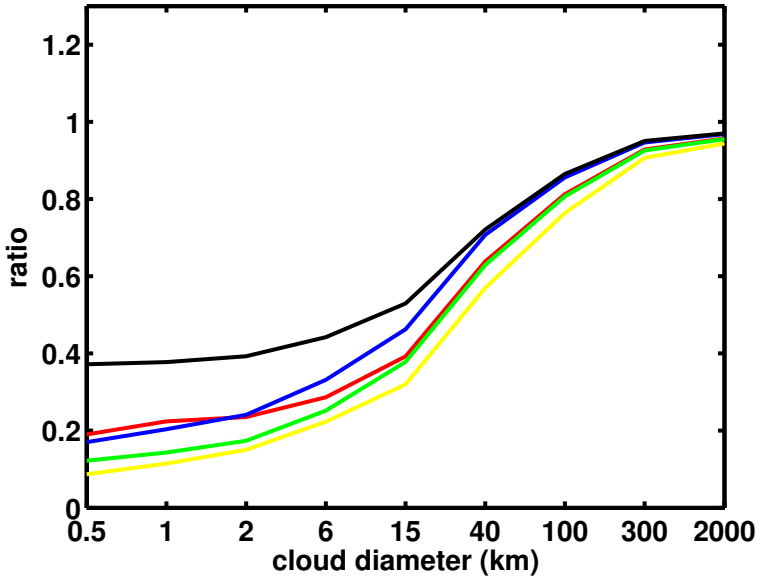

Fig. 4. Horizontal-size dependence of $\widehat{R}_{\mathrm{col}}^{\mathrm{cloud}}/R_{\mathrm{col}}^{\mathrm{cloud}}$ for different types of clouds: cumulus and stratocumulus (1–2 km, red), altostratus (3–5 km, green), altocumulus (2–3 km, blue), nimbostratus (2–5 km, yellow), cirrus (8–9.5 km, black).

ACPD
14, 9815–9847, 2014

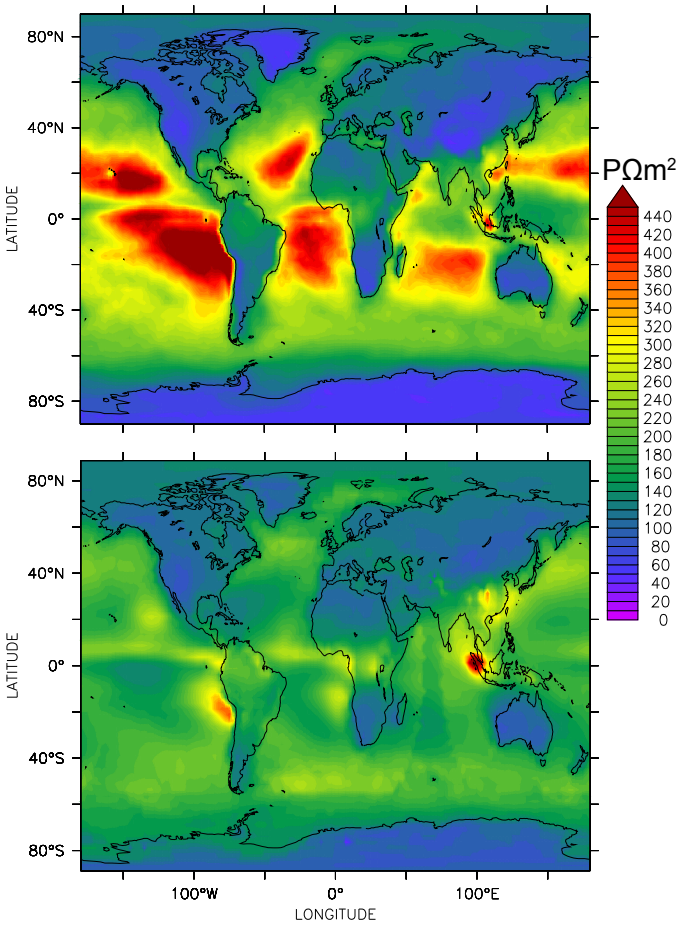

Fig. 5. CESM1(WACCM) (top) and ISCCP (bottom) average column resistance, taking the current divergence/convergence phenomenon into account ($\eta = 1/50$).

ACPD
14, 9815–9847, 2014

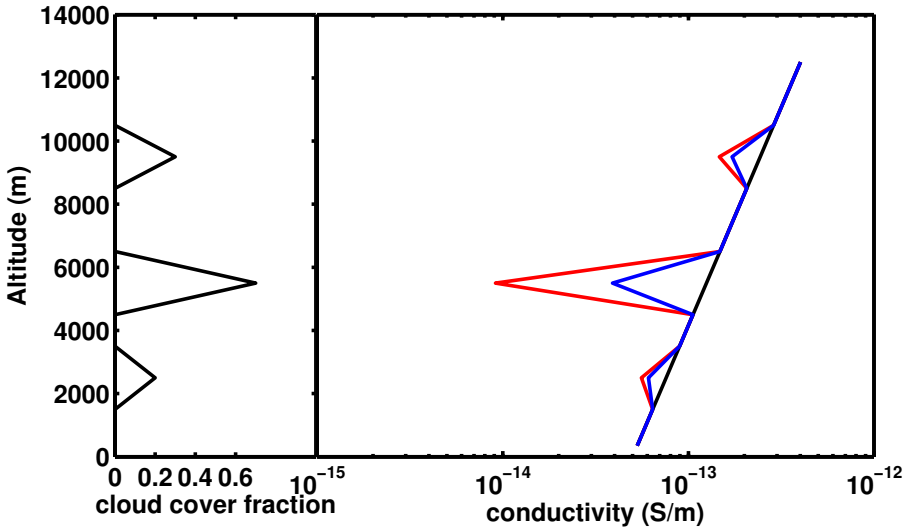

Fig. 6. Left: cloud cover fraction of a single column. Right: Background (black), ZT10 (blue) and parameterized (red, see text) cloud conductivity profile.

ACPD
14, 9815–9847, 2014

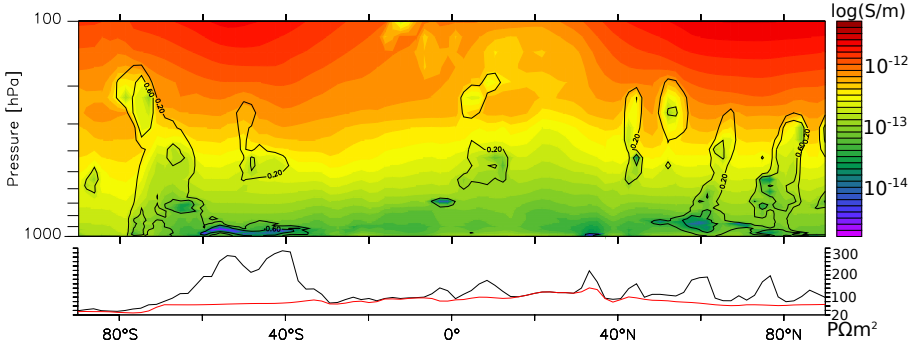

Fig. 7. Top: Logarithm of conductivity from CESM1(WACCM) for 30° E and 16 September 2005, 00:00 UTC, using the cloud conductivity parametrization. The black contour lines indicate cloud cover fraction. Bottom: column resistance for the same location, using the cloud parametrization (black) and neglecting clouds (red).

ACPD
14, 9815–9847, 2014

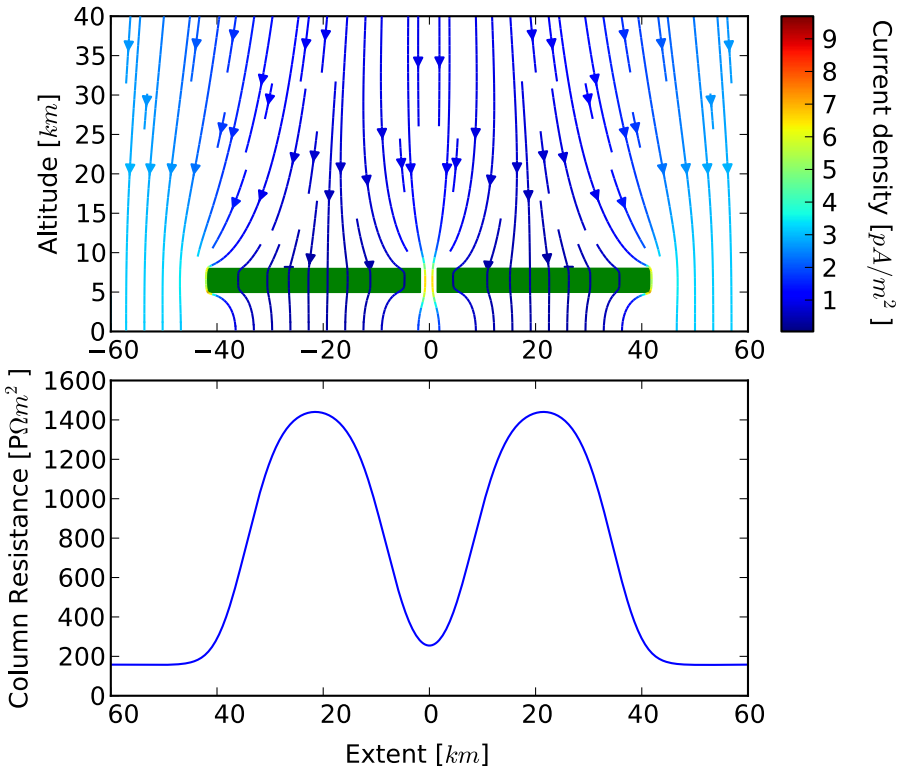

Fig. 8. Top: Current streamlines in the vicinity of two clouds that are separated by 3 km. Bottom: corresponding column resistance $\widehat{R}_{\text{col}}$.

ACPD
14, 9815–9847, 2014